AGU PUBLICATIONS

JGR

Journal of Geophysical Research: Space Physics

RESEARCH ARTICLE
10.1002/2016JA023070

Key Points:
- Parametric instability is excited by *X*-mode pump wave heating
- HFPLs and HFILs are observed by EISCAT radar
- Physical mechanisms are summarized

Correspondence to:
C. Zhou,
chenzhou@whu.edu.cn

Citation:
Wang, X., C. Zhou, M. Liu, F. Honary, B. Ni, and Z. Zhao (2016), Parametric instability induced by *X*-mode wave heating at EISCAT, *J. Geophys. Res. Space Physics*, *121*, 10,536–10,548, doi:10.1002/2016JA023070.

Received 15 JUN 2016
Accepted 6 OCT 2016
Accepted article online 8 OCT 2016
Published online 26 OCT 2016

Parametric instability induced by *X*-mode wave heating at EISCAT

Xiang Wang[1,2], Chen Zhou[1], Moran Liu[1], Farideh Honary[2], Binbin Ni[1], and Zhengyu Zhao[1]

[1]Department of Space Physics, School of Electronic Information, Wuhan University, Wuhan, China, [2]Department of Physics, Lancaster University, Lancaster, UK

Abstract In this paper, we present results of parametric instability induced by *X*-mode wave heating observed by EISCAT (European Incoherent Scatter Scientific Association) radar at Tromsø, Norway. Three typical *X*-mode ionospheric heating experiments on 22 October 2013, 19 October 2012, and 21 February 2013 are investigated in details. Both parametric decay instability (PDI) and oscillating two-stream instability are observed during the *X*-mode heating period. We suggest that the full dispersion relationship of the Langmuir wave can be employed to analyze the *X*-mode parametric instability excitation. A modified kinetic electron distribution is proposed and analyzed, which is able to satisfy the matching condition of parametric instability excitation. Parallel electric field component of *X*-mode heating wave can also exceed the parametric instability excitation threshold under certain conditions.

1. Introduction

The ionospheric modification experiments by ground-based high powerful high-frequency (HF, 3–30 MHz) electromagnetic (EM) heating wave have been performed all over the world since 1970s [*Fialer*, 1974; *Minkoff et al*., 1974; *Robinson*, 1989; *Thome and Blood*, 1974; *Utlaut and Cohen*, 1971]. The ionospheric heating has been an active plasma experimental platform to investigate the process of nonlinear wave-particle and wave-wave interaction [*Leyser and Wong*, 2009]. The principal phenomena of ionospheric heating experiments include large-scale ionospheric temperature and density change, HF-enhanced plasma lines (HFPLs), stimulated electromagnetic emissions (SEEs) [*Stubbe et al*., 1984], enhanced airglow [*Bernhardt et al*., 1989; *Kosch et al*., 2002, 2007a, 2007b; *Pedersen and Carlson*, 2001; *Blagoveshchenskaya et al*., 2014], Langmuir turbulence [*DuBois et al*., 1990; *Stubbe et al*., 1992; *Gurevich et al*., 2004], and artificial field-aligned irregularities [*Grach and Trakhtengerts*, 1975]. The associated physical mechanisms such as ohmic absorption, self-focusing instability, and parametric instability have been proposed and discussed by many researchers [*Robinson*, 1989; *Gurevich*, 2007; *Kosch et al*., 2007c; *Gondarenko et al*., 2006].

The large amplitude HF heating wave can act as a pump wave to excite plasma intrinsic modes through parametric coupling. This parametric instability process provides effective way to convert ground-transmitted electromagnetic heating waves into plasma waves, which can be directly observed by UHF/VHF incoherent scatter radars. The UHF/VHF radars transmit the radio wave signal and receive returned echoes backscattered by the plasma waves. The wave vector and frequency of the radar scatter are imposed by the Bragg scattering conditions: $\vec{k}_S = \vec{k}_R \pm \vec{k}_P$ and $\omega_S = \omega_R \pm \omega_P$, where the subscripts *R*, *S*, and *P* represent the incident radar wave, the radar scatter, and the plasma wave, respectively. $\vec{k}$ is the wave vector and ω is the wave angular frequency. Thus, the Doppler width of the returned spectrum $(\omega_R - \omega_S)$ is related to the frequencies of the plasma waves $\mp\omega_P$. Since $\vec{k}_S = -\vec{k}_R$ for backscatter, $\vec{k}_P = \mp 2\vec{k}_R$. Thus, the wavelength of the plasma wave observed by UHF/VHF radar has to be half of the radar wave and to propagate parallel or antiparallel to the radar beam. The parallel and antiparallel propagating plasma waves generate radar returns with positive and negative Doppler shifts. The enhanced spectral lines on the negative side correspond to upgoing plasma waves and those on the positive side correspond to downgoing plasma waves. These plasma spectra lines are named as HF-enhanced plasma lines for electron plasma waves and HF-enhanced ion lines (HFILs) for ion acoustic waves. Besides, phenomena such as airglow enhancement, short-scale (meters) field-aligned density irregularities, and SEEs are all ascribed directly or indirectly to the excitation of parametric instabilities.

Parametric decay instability (PDI) and oscillating two-stream instability (OTSI) excited by the ordinary polarization (*O* mode) heating wave have been investigated extensively since the *O*-mode wave can satisfy the

matching condition of parametric excitation [*Fejer*, 1979; *Perkins et al*., 1974; *Kuo*, 1996, 2002, 2015]. The amplified parallel electric field of the *O*-mode heating wave near the reflection region is the dominant factor for parametric instability excitation [*Fejer*, 1979; *Kuo*, 2015]. *Freund and Papadopoulos* [1980] analyzed the threshold and growth rate of the PDI and OTSI in a weakly magnetic field under condition $\omega_0 << k_{\parallel} v_{Te}$ (where ω_0, $k_{\parallel}$, and v_{Te} are the heating wave angular frequency, longitudinal wave number of high-frequency Langmuir wave, and electron thermal speed, respectively.). Since the plasma frequency at the extraordinary polarized (*X* mode) heating wave reflection height is less than the heating wave frequency, which cannot satisfy the frequency matching condition of parametric instability excitation. The *X*-mode heating wave is generally considered not be able to excite Langmuir wave or upper hybrid wave near *X*-mode wave reflection height [*Lee and Kuo*, 1983; *Kuo*, 2015]. In addition, the parallel electric field of *X*-mode wave at the reflection height is negligible [*Ginzburg*, 1970], which do not exceed the threshold parallel electric field.

However, observations of the *X*-mode heating experiments indicate that *X*-mode heating wave is also capable of producing abundant phenomena, including the HFPLs and HFILs. *Fejer and Leer* [1972] presented that the electron Bernstein mode may be excited parametrically by the extraordinary heating wave with multigyrofrequency near the *X*-mode heating wave reflection height. *Vas'kov and Ryabova* [1998] demonstrated that the upper hybrid (UH) waves can also be excited by *X*-mode heating through PDI near the reflection height and the excitation threshold was estimated as ~1.35 V/m under the condition $\omega_0/\Omega_e = 4.5$, where Ω_e is the electron gyrofrequency. Recently, *Blagoveshchenskaya et al*. [2011, 2013] reported the observations of the field-aligned irregularities and the change of large-scale electron density and temperature during the *X*-mode heating experiments. *Senior et al*. [2013] presented evident large electron density enhancement during both *O*- and *X*-mode heating periods at European Incoherent Scatter Scientific Association (EISCAT) and revealed that only the *X*-mode heating wave with higher frequency can excite HFILs and HFPLs. By using the EISCAT observations, *Blagoveshchenskaya et al*. [2014] presented the HFPLs and zero-frequency offset HFILs during the *X*-mode heating periods. The HFPLs are related to the excited Langmuir wave propagating along the radar beam, while the zero-frequency offset HFILs indicate the excitation of the OTSI. The behavior of enhanced airglow generated by *X*-mode EM heating wave at Tromsø, Norway, has also reported and compared to the *O*-mode heating experiments [*Blagoveshchenskaya et al*., 2014].

The purpose of this study is to investigate the parametric instability excited by *X*-mode heating wave. By analyzing the observations from EISCAT (European Incoherent Scatter Scientific Association) radar, we aim to explain the potential mechanism for parametric instability excitation and to understand the physical factors accounting for the parametric instability induced by *X*-mode heating wave. The outline of this paper is as follows. In section 2, three typical experiments of parametric instability with HFPLs and HFILs observed by EISCAT UHF radar are analyzed in details. In sections 3, we further discuss the potential interpretation for the observed parametric instability induced by *X*-mode heating wave. The threshold electric field for parametric instability excited by *X*-mode heating wave is also investigated. The principal conclusions are summarized in section 4.

2. Observations of EISCAT

Here we report three *X*-mode heating experiments operated on 19 October 2012 and 21 February and 22 October 2013, which provide direct evidence to support the excitation of parametric instability by *X*-mode EM heating wave.

The EISCAT UHF radar is able to observe the longitudinal Langmuir wave (LW) and ion acoustic wave (IAW). A strong LW and IAW are directly attributed to parametric instability excited by the high-frequency (HF) heating wave near the heating wave reflection height. Both IAW and LW are directly detected by EISCAT UHF radar near the heating facility as HF-enhanced ion and plasma lines in the radar spectra. Here we report the distribution of HFILs and downshifted HFPLs in the frequency band corresponding to the LW and IAW. We highlight one point is that the EISCAT UHF radar is only able to detect the downshifted HF-induced plasma lines [*Senior et al*., 2013]. The HFILs and downshifted HFPLs are calculated by the Grand Unified Incoherent Scatter Design and Analysis Package (Guisdap) [*Lehtinen and Huuskonen*, 1996]. The temporal-altitude variation of the background plasma parameters is also calculated by Guisdap from the EISCAT UHF radar observed data, such as the electron temperature and electron density. By taking into account the *D* region absorption [*Senior et al*., 2010], the effective radiated power (ERP) of the heating wave in the magnetic zenith direction is calculated according to different heating wave frequencies and different experimental time.

2.1. Case 1

The first experiment is carried out on 22 October 2013 [*Blagoveshchenskaya et al*., 2014]. The heater wave frequency 7.1 MHz is below the critical frequency of F_2 layer (f_oF_2) during the whole heating periods. In this experiment, an *X*-mode heating wave is transmitted from 15:31 UT to 17:58 UT with sequence of 10 min on and 5 min off. The equivalent effective radiated power (ERP) of the *X*-mode heating wave in the magnetic zenith is estimated about 548 MW. Both the *X*-mode heating wave and the UHF radar beam point along the magnetic field-aligned direction. The heating sequence and estimated heating ERP are illustrated in Figure 1a. During the whole heating period of this experiment, the HFPLs and HFILs were observed during all 10 min heater on cycle. The HFPLs and HFILs observed by the EISCAT UHF radar are presented in Figures 1b–1f. Figures 1b and 1c illustrate the downshifted HFPLs and the altitude-temporal behavior of the downshifted HFPLs during the heating period. Strong downshifted HFPLs at about −7.1 MHz shown in Figure 1b indicate the excited upward Langmuir wave by parametric instability. Figure 1c demonstrates the temporal change of the height of Langmuir wave excitation during the heating periods. Figure 1d demonstrates the downshifted HFILs near the *X*-mode reflection height (the blue solid line in Figure 1g). The altitude-temporal variations of the downshifted HFILs are shown in Figure 1e. Figure 1f presents the altitude-temporal variations of upshifted HFILs at the *O*-mode reflection height. The reflection height of the *X*-mode heating wave is calculated according to $\omega_{pe}^2 = \omega_0(\omega_0 - \Omega_e)\cos^2\alpha$ [*Ginzburg*, 1970], where ω_0, ω_{pe}, and Ω_e are the angular frequency of the heating wave, the local electron plasma frequency and the electron gyrofrequency, respectively; $\alpha = 12°$ is the complement of the local dip angle. As shown in Figure 1e, downshifted HFILs appear in two different height ranges. One is around 225 km where it is near the reflection height of the *X*-mode heating wave (the blue solid line in Figure 1g), and the other is near the reflection altitude of the *O*-mode heating wave (the red solid line in Figure 1g), where $\omega_{pe}^2 = \omega_0^2\cos^2\alpha$ [*Ginzburg*, 1970]. Figure 1g displays the temporal-altitude behavior of the electron temperature measured by the EISCAT UHF radar during the heating period. The increase of the electron temperature is observed in the heater on cycle.

Since the ground-based HF transmitter at Tromsø, Norway, cannot separate the *O*-mode and *X*-mode wave absolutely [*Blagoveshchenskaya et al*., 2014], the leakage of *X*-mode power to *O*-mode is feasible. In this case, the HFPLs and HFILs at *O*-mode reflection height are also observed during the *X*-mode heating sequence. *Blagoveshchenskaya et al*. [2014] suggested that less than 1% of full ERP could be leaked to *O*-mode wave under *X*-mode heating wave. However, in this case, at least 2%–3% ERP of *X*-mode leakage to *O*-mode wave is estimated to excite the HFPLs and HFILs.

Although we cannot separate the HFILs and HFPLs excited by *O*- or *X*-mode in the spectrum due to the power leakage problem, we can still distinguish the parametric instability excited by *O*-mode/*X*-mode heating waves according to the different excitation heights. As shown in Figure 1e, two separated lines can be observed at two different heights, which indicate that two ion acoustic waves are excited simultaneously at the reflection heights of the *O*-mode and *X*-mode heating waves. The downshifted HFILs excited by *X*-mode heating waves presented in Figures 1d and 1e indicate the upward propagation IAW. According to the wave vector matching condition (equation (4)), a corresponding downward LW (upshifted HFPL) should also be excited. However, due to the technical limitations of the EISCAT UHF radar, the upshifted plasma lines cannot be measured.

2.2. Case 2

An alternative sequence of *O*-mode/*X*-mode heating wave experiment is carried out on 19 October 2012. The experiment is performed from 17:01 UT to 18:58 UT with 10 min on and 5 min off cycle. From 17:01 UT to 18:01 UT, the heating frequency is 6.2 MHz and the ERP during this period changes from 458 MW to 383 MW at 17:46 UT due to one heating transmitter switch-off, as shown in Figure 2a. From 18:01 UT to 18:58 UT, the heating wave frequency is 5.423 MHz with ERP of 300 MW. Figure 2b illustrates the spectrum of the downshifted HFPLs during the heating period. The temporal-altitude variations of the downshifted HFPLs are shown in Figure 2c. The temporal-altitude variations of the HFILs are shown in Figure 2d. The temporal-altitude variation of downshifted, zero-frequency offset, and upshifted HFILs is shown in Figures 2e–2g, respectively. The temporal-height variation of the electron temperature is shown in Figure 2h. The reflection height of the heating wave are $\omega_{pe}^2 = \omega_0^2\cos^2\alpha$ for the *O*-mode wave (the red solid line in Figure 2h)

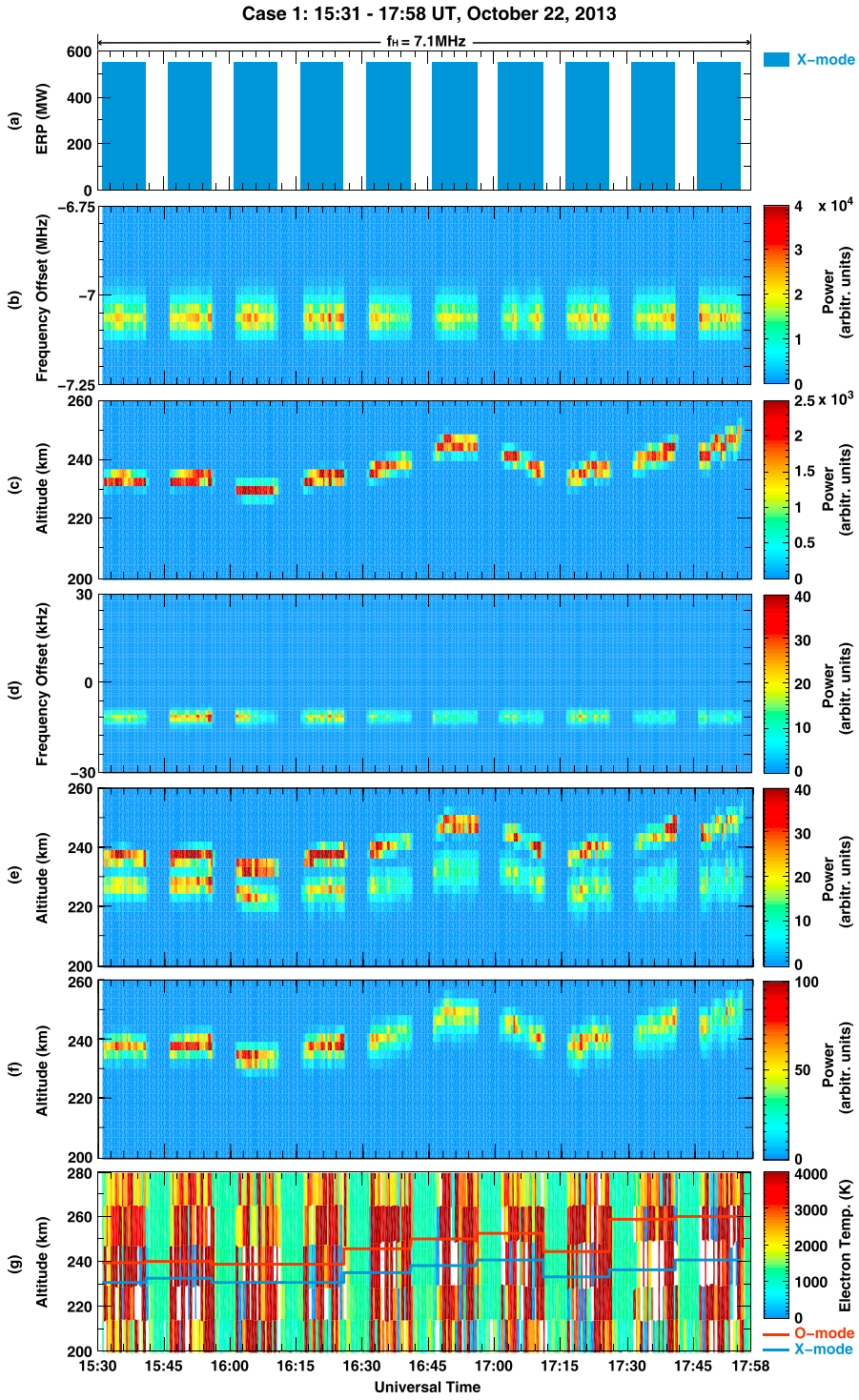

Figure 1. Ionospheric heating experiment at Tromsø from 15:31 UT to 17:58 UT on 22 October 2013 (a) Heater wave consequence and temporal variation of ERP, (b) temporal variations of the undecoded downshifted plasma line in the range of altitudes of 128–302 km with 30 s integration time, (c) temporal-altitude behavior of the undecoded downshifted plasma line with 3 km range resolution and 30 s integration time, (d) temporal variation of HF-induced ion line near reflection height of the pump wave with 30 s integration time, (e) temporal-altitude behavior of the downshifted ion line spectra at −11.9 kHz, (f) temporal-altitude behavior of the upshifted ion line spectra at +11.9 kHz, (g) temporal-altitude behavior of the electron temperature and the solid lines mark the reflection height of the *O*-mode (red) and the *X*-mode (blue) heating wave. The plasma line intensity, ion line intensity, and the electron temperature are obtained from the EISCAT UHF radar observation during the heating experiment with 10 min on and 5 min off cycle.

and $\omega_{pe}^2 = \omega_0(\omega_0 - \Omega_e)\cos^2\alpha$ for *X*-mode wave (the blue solid line in Figure 2h) [*Ginzburg*, 1970]. Strong HFPLs can be observed in Figures 2b and 2c during 17:16–17:26 UT during the 6.2 MHz *X*-mode heating sequence. The strong HFPLs at about 250 km shown in Figure 2c during the *X*-mode heating period (17:16–17:26 UT) indicate that the Langmuir wave is parametrically excited by the *X*-mode heating wave. Besides, strong downshifted and upshifted HFILs with the weak zero-frequency offset HFILs during the same *X*-mode heating period are also observed, as seen in Figure 2d. The zero-frequency offset HFILs indicate the excitation of the OTSI. As the heating wave frequency decreased to 5.423 MHz from 18:01 to 18:58 UT, the ERP of heating transmitter dropped to 300 MW. However, the weak HFPLs and HFILs are still observed in Figures 2b and 2d during the *X*-mode heating period 18:01–18:11 UT. Although the corresponding HFPLs is not seen obviously in Figure 2c, we should mention that the measurement data dump still contains an enhanced plasma line with amplitude of 3.67 (arbitrary unit), which is not negligible comparing to noise level. During the whole heating period, *O*-mode heating wave did not produce obvious HFPLs and HFILs.

2.3. Case 3

Another heating experiment is conducted on 21 February 2013. Figure 3a demonstrates the alternative *O*-mode/*X*-mode sequence from 12:01 to 15:31 UT on 21 February 2013. During the 12:01–14:26 UT, the frequency of heating wave is 7.1 MHz with ERP of 529 MW. From 14:31 UT to 15:31 UT, the frequency of heating wave is 5.423 MHz and the ERP is 310 MW. The heating sequence is 10 min on and 5 min off cycle. According to the nearby ionosonde records, the *O*-mode heating wave penetrates out the ionosphere from 12:01 UT to 14:26 UT, which is the under dense heating. The *X*-mode heating wave penetrates out the ionosphere at heating cycle of 14:16–14:26 UT due to the background ionospheric change. Figures 3b and 3c demonstrate the observed downshifted HFPLs and temporal-altitude variation of the downshifted HFPLs, respectively. Strong HFPLs can be observed at *X*-mode heating period, while no obvious plasma lines are observed during the *O*-mode heating cycle. Since the *X*-mode wave penetrates the ionosphere at period of 14:16–14:26 UT, no HFPLs are observed at this period. Figure 3d shows the temporal behavior of the HFILs near the reflection height of the *X*-mode heating wave. Figures 3e–3g illustrate the temporal-altitude variation of the downshifted, zero-frequency offset, and upshifted HFILs, respectively. During the first four *X*-mode heating periods with frequency of 7.1 MHz, strong HFILs are observed near the reflection height of the *X*-mode heating wave (the blue solid line in Figure 3h), with the corresponding strong HFPLs at the same height. Since in the last heating periods of *X*-mode with frequency of 7.1 MHz, the heating wave penetrates the ionosphere, which is the under dense heating situation. No obvious HFILs are observed during 14:16–14:26 UT *X*-mode heating period. Ascending and descending echoes of the HFPLs and the HFILs are observed at *X*-mode heating periods of 13:16–13:26 UT and 13:46–13:56 UT in Figures 3c and 3e–3g. These ascending and descending structures have also been reported and discussed by *Pedersen et al*. [2009] and *Mishin et al*. [2016].

When the heating wave frequency is 5.423 MHz, both the strong HFILs and HFPLs are observed at *X*-mode heating cycle. Since the *O*-mode heating frequency is close to the fourth electron gyrofrequency, it is noted that the ion lines spectrum was considerably enhanced near the reflection height of the *O*-mode wave (the red solid line in Figure 3h) during the *O*-mode heating period of 14:31–14:41 UT, yet without the presence of corresponding HFPLs. This phenomenon has also been presented by *Honary et al*. [1999] and *Ashrafi et al*. [2007]. Figure 3h presents the temporal-altitude variation of electron temperature. The electron temperature increases in every cycle of heater switching on.

3. Discussions

The ionospheric modification experiments presented above provide direct evidence that the parametric instability is excited during *X*-mode heating period. Table 1 summarizes the parametrically excited plasma waves observed in the three cases. The HFPLs and HFILs observed during the *X*-mode heating period indicate the excitation of PDI. The zero-frequency offset enhanced ion lines observed during *X*-mode heating period in Case 2 and Case 3 indicate the excitation of OTSI.

3.1. Matching Condition of Parametric Instability

When a high powerful HF electromagnetic wave $\vec{E}_p\left(\omega_0, \vec{k}_0\right)$ injects into the ionospheric plasma, it acts as a pump wave to excite high- and low-frequency plasma waves simultaneously via the parametric coupling

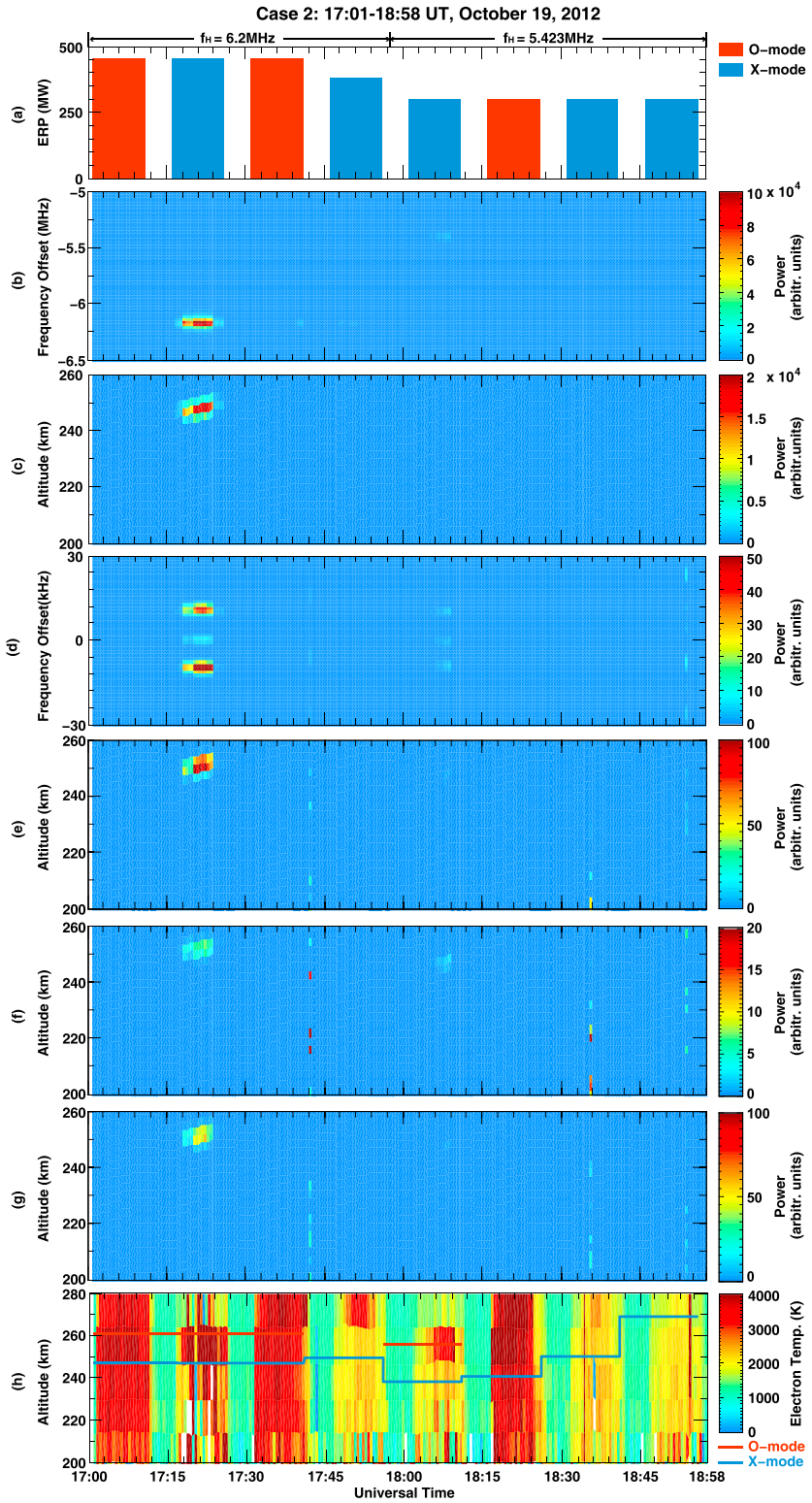

Figure 2. Ionospheric heating experiment at Tromsø from 17:01 UT to 18:58 UT on 19 October 2012. (a–d) Same format as Figure 1, (e) temporal-altitude behavior of the downshifted ion line spectra at −9.5238 kHz, (f) temporal-altitude behavior of the zero-frequency ion line spectra, (g) temporal-altitude behavior of the upshifted ion line spectra at +9.5238 kHz, (h) temporal-altitude behavior of the electron temperature and the solid lines mark the reflection height of the *O*-mode (red) and the *X*-mode (blue) heating wave. The plasma line intensity, ion line intensity, and the electron temperature are obtained from the EISCAT UHF radar observation during the heating experiment with 10 min on and 5 min off cycle.

process. For the PDI, the heating wave decays to a high-frequency Langmuir wave $\left(\omega_{LW}, \vec{k}_{LW}\right)$ and a low-frequency ion acoustic wave $\left(\Delta\omega_{IAW}, \Delta\vec{k}_{IAW}\right)$. For the OTSI, the HF heating wave decays to two oppositely propagating high-frequency Langmuir waves $\left(\omega_{LW}, \vec{k}_{LW}\right)$ and $\left(\omega'_{LW}, \vec{k}_{LW}{}'\right)$ together with a purely growing mode $\left(\Delta\omega_{PM}, \Delta\vec{k}_{PM}\right)$. The frequencies and wave vectors of the excited plasma waves are governed by the matching condition:

$$\begin{aligned} \omega_0 &= \omega_{LW} + \Delta\omega_{IAW} \\ \omega_0 &= \omega_{LW} + \Delta\omega_{PM}{}^* = \omega'_{LW} - \Delta\omega_{PM} \end{aligned} \tag{1}$$

$$\begin{aligned} \vec{k}_0 &= \vec{k}_{LW} + \Delta\vec{k}_{IAW} \\ \vec{k}_0 &= \vec{k}_{LW} + \Delta\vec{k}_{PM} = \vec{k}_{LW}{}' - \Delta\vec{k}_{PM}, \end{aligned} \tag{2}$$

where ω_{LW}, ω'_{LW} and $\vec{k}_{LW}$, $\vec{k}_{LW}{}'$ are the wave frequency and wave vector of the high-frequency Langmuir waves; $\Delta\omega_{IAW}$ and $\Delta\vec{k}_{IAW}$ represent the frequency and wave vector of the low-frequency ion acoustic waves; $\Delta\omega_{PM}$ and $\Delta\vec{k}_{PM}$ are the wave frequency and wave vector of the purely growing mode.

The wave number of the EM heating wave can be approximately obtained from the following equation $k_0 = n_p\omega_0/c$, where c is the speed of light and n_p is the refractive index of the heating wave. Since the value of k_0 is almost zero near the reflection height of heating wave and for purely growing mode $\mathrm{Re}(\Delta\omega_{PM}) = 0$. Thus, the frequency matching condition (1) and wave vector matching condition (2) can be rewritten as

$$\text{For PDI}: \quad \begin{aligned} \omega_0 &= \omega_{LW} + \Delta\omega_{IAW} \\ \vec{k}_{LW} &= -\Delta\vec{k}_{IAW} \end{aligned} \tag{3}$$

$$\text{For OTSI}: \quad \begin{aligned} \omega_0 &= \mathrm{Re}(\omega_{LW}) = \mathrm{Re}\left(\omega'_{LW}\right) \\ \vec{k}_{LW} &= -\vec{k}_{LW}{}' = -\Delta\vec{k}_{PM} \end{aligned} \tag{4}$$

For the typical Maxwellian distribution, the dispersion relation of parallel Langmuir wave is

$$\mathrm{Re}(\omega_{LW}) = \sqrt{\omega_{pe}^2 + \gamma_e k^2 v_{the}^2} \tag{5}$$

where k is the wave number of the Langmuir wave and γ_e is the adiabatic index for electron; in the ionosphere $\gamma_e = 3$. For the *O*-mode heating wave, the reflection height is at where $\omega_{pe} = \omega_0\cos\alpha$; for the *X*-mode heating wave in our cases, the reflection height is at where $\omega_{pe}^2 = \omega_0(\omega_0 - \omega_{ce})\cos^2\alpha$. For a heating wave with frequency ω_0, matching conditions (3) and (4) and expression (5) determine the height where PDI/OTSI is excited. This height is slightly lower than the *O*-mode wave reflection height yet higher than *X*-mode reflection height, hence making PDI excitation by *X*-mode heating wave impossible [*Perkins et al*., 1974; *Kuo*, 2015]. Take the experiment performed with $f_H = 6.2$ MHz on 19 October 2012 for example. The wave number of the excited Langmuir wave and ion acoustic wave equals the twice wave number of the 930 MHz EISCAT UHF radar due to Bragg scattering condition, i.e., $k \approx 2k_R \approx 12.44\pi$. The undisturbed ionospheric parameters are obtained from the UHF radar measurements, as shown in Table 2. It is obtained the following values: Ion acoustic speed $c_s = 1.532 \times 10^3$m/s, ion acoustic wave frequency $\omega_{\mathrm{IAW}} = kc_s = 2\pi \times 9.53$ kHz, electron thermal speed $v_{Te} = 1.332 \times 10^5$m/s, electron plasma frequency $\omega_{pe} = 2\pi \times 5.4826$ MHz. Taking into account the frequency resolution with 2.9311 kHz in the ion line spectra, the observed ion acoustic wave frequency ±9.5238 kHz is agree with the calculation results, which indicate the dispersion relation of the IAW is satisfied. However, taking the above values into the dispersion relation of the LW (equation (5)), the real part of Langmuir wave frequency equals $2\pi \times 5.6682$ MHz, which is far away from the frequency of the observed Langmuir wave ($f_{\mathrm{LW}} = 6.1998$ MHz for OTSI and $f_{\mathrm{LW}} = 6.1888$ MHz for PDI). However, the observations presented in section 2 indicate that *X*-mode heating wave is also capable of exciting the parametric instability. Taking Figure 3b, for example, the frequency of downshifted HFPLs is around −7.0908 MHz, close to the

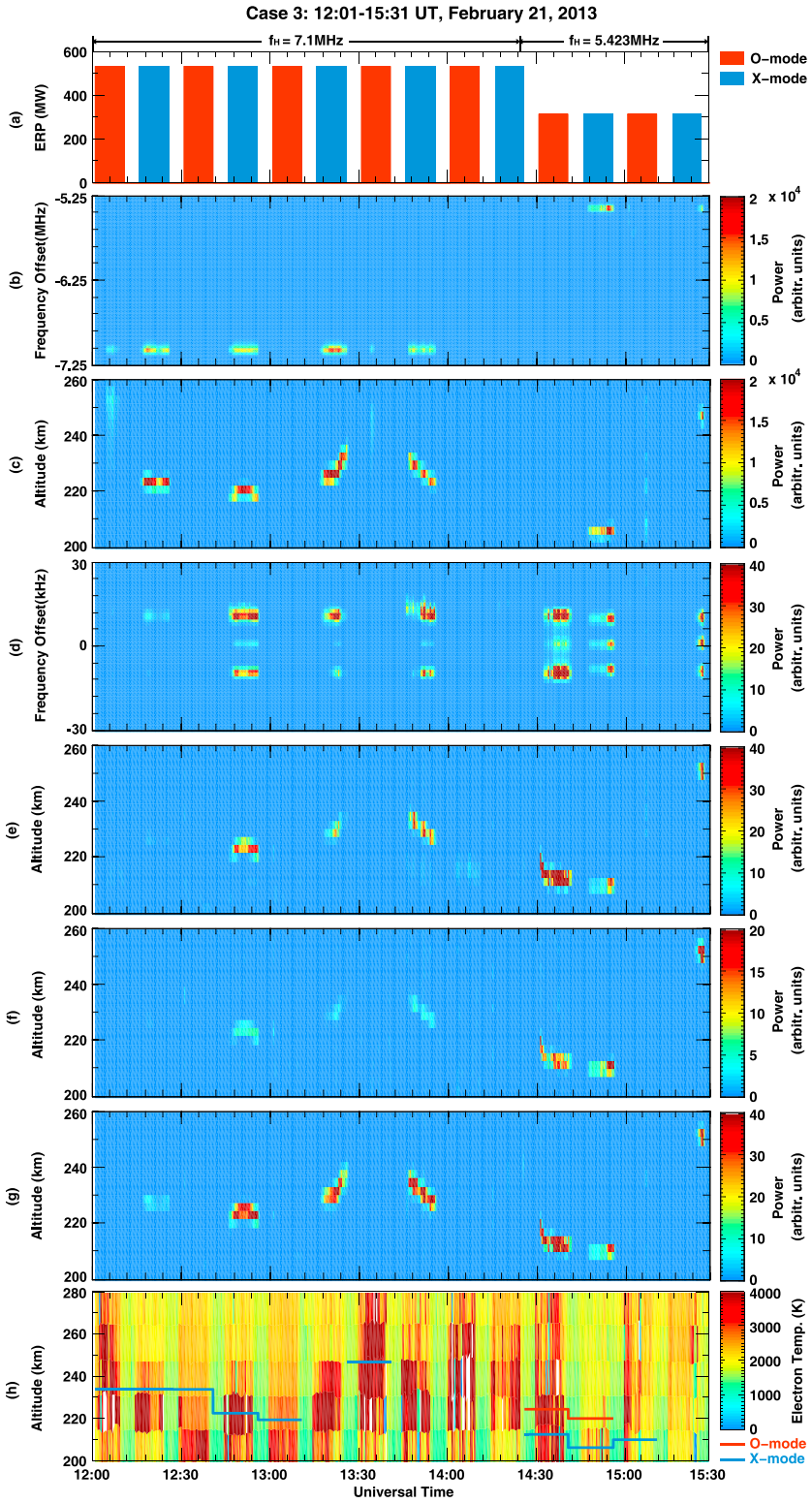

Figure 3. Ionospheric heating experiment at Tromsø from 12:01 UT to 15:31 UT on 21 February 2013 (a–d and f) Same format as Figure 1, (e) temporal-altitude behavior of the downshifted ion line spectra at −9.624 kHz, (f) temporal-altitude behavior of the zero-frequency ion line spectra, (g) temporal-altitude behavior of the upshifted ion line spectra at +9.624 kHz, (h) temporal-altitude behavior of the electron temperature and the solid lines mark the reflection height of the *O*-mode (red) and the *X*-mode (blue) heating wave. The plasma line intensity, ion line intensity, and the electron temperature are obtained from the EISCAT UHF radar observation during the heating experiment with 10 min on and 5 min off cycle.

Table 1. Summary for the Observed HFILs and HFPLs in the Three Cases[a]

	Case 1		Case 2		Case 3	
Experiments	*O*-mode	*X*-mode	*O*-mode	*X*-mode	*O*-mode	*X*-mode
Downshifted HFPLs[c]	√	×	×	√	×	√
Downshifted HFILs	√	√	×	√	√[b]	√
Upshifted HFILs	√	×	×	√	√[b]	√
Zero-offset HFILs	×	×	×	√	√[b]	√

[a]√—observed and ×—absence.
[b]Enhanced HFILs are observed at *O* mode with the frequency of 5.423 MHz, close to the fourth electron gyrofrequency.
[c]Upshifted plasma line is not measured due to technical limitations of the UHF radar [*Senior et al.*, 2013].

heater wave frequency; while the frequency of downshifted HFILs is about −9.624 kHz in Figure 3d, which is close to the ion acoustic wave frequency. This is a direct evidence of the satisfaction of frequency mating condition and the excitation of PDI. The *X*-mode heating wave decays to a Langmuir wave and an ion acoustic wave near the reflection altitude of the *X*-mode heating wave. For Case 2, the frequency offset of HFPLs is observed at −6.1888 MHz and −6.1998 MHz and the corresponding downshifted HFILs (−9.5238 kHz), upshifted HFILs (+9.5238 kHz), and HFILs of zero-frequency offset is observed from 17:16–17:26 UT. The enhanced ion lines spectra at zero-frequency offset indicate the excitation of OTSI.

Thus, we suggest that the matching condition can be satisfied near the reflection height of *X*-mode heating wave by considering the kinetic modified dispersion relation of Langmuir wave. If the full dispersion relation [*Baumjohann and Treumann*, 1996] by assuming electrostatic waves and parallel propagation is taken into consideration, the frequency of Langmuir wave, excited by the *X*-mode heating wave via the parametric instability, can be obtained.

$$\omega^2_{\text{Langmuir}}(k,\theta) = \omega_p^2 + \omega_{pe}^2 \int_0^\infty 2\pi v_\perp dv_\perp \int_{-\infty}^{\infty} \frac{k_\parallel {v_\parallel}^2 \partial f/\partial v_\parallel}{\omega_{\text{Langmuir}} - k_\parallel v_\parallel} dv_\parallel, \tag{6}$$

where $\omega_p = (n_e e^2/\varepsilon_0 m_p)^{1/2}$ is the plasma frequency, m_p is the effective plasma mass which depends on ion components and electron in the plasma, θ is the angle between the wave vector $\vec{k}$ and the magnetic field $\vec{B}_0$, and f is the electron distribution function. By considering this relation, the excitation height of PDI/OTSI can be lower to the reflection height of the *X*-mode heating wave. Consequently, the matching condition can be satisfied by *X*-mode heating wave. In this paper, it is assumed that the ion velocity satisfies the Maxwellian distribution function. The ion acoustic wave frequency adopts the standard long wave approximation, i.e., $\omega_{IAW} = kc_s$ [*Brambilla*, 1998], because the condition $k\lambda_D << 1$ is satisfied in the heating experiments, where λ_D is the electron Debye length.

For further analyze equation (6), take the modified bi-Maxwellian distribution [*Mishin et al.*, 2000] as the electron velocity distribution function as an example:

$$f(v_\parallel, v_\perp) = \frac{\kappa n_0}{\pi^{3/2} v_{Te\parallel} v_{Te\perp}^2} \exp\left(-\frac{{v_\parallel}^2}{v_{Te}^2\parallel} - \frac{v_\perp^2}{v_{Te\perp}^2}\right), \tag{7}$$

where $\kappa = \frac{\omega_0}{\omega_0 - \Omega_e}$, $v_\parallel$, $v_\perp$, $v_{Te\parallel}$, and $v_{Te\perp}$ are the parallel electron velocity, the perpendicular electron velocity, the parallel electron thermal velocity, and the perpendicular electron thermal velocity, respectively. Here both the parallel and the perpendicular direction are with respect to the magnetic field.

Taking the equation (7) into equation (6), we can obtain the real part of the Langmuir wave frequency as the below:

$$\omega_{LW}^2 = \omega_{pe}^2 \kappa \Lambda_0(\eta_e) \cos^2\theta \left(1 + 3k^2\lambda_D^2 \cos^2\theta\right), \tag{8}$$

where $\Lambda_0(\eta_e) = I_0(\eta_e)\exp(-\eta_e)$, $\eta_e = k_\perp^2 v_{Te}^2/2\Omega_e^2$, I is modified Bessel function, and $\lambda_D = (\varepsilon_0 k_b T_e/n_0 e^2)^{1/2}$ is the electron Debye length. Equation (8) is the modified dispersion relation of the Langmuir wave, which is adopted to explain the satisfaction of the frequency matching condition near the *X*-mode reflection height.

Table 2. The Threshold Field for Three Experiments

Experiments	Case 1	Case 2		Case 3	
Heating wave frequency	7.1 MHz	6.2 MHz	5.423 MHz	7.1 MHz	5.423 MHz
PDI threshold field	0.12 V/m	0.10 V/m	0.10 V/m	0.12 V/m	0.24 V/m
Equivalent ERP of PDI threshold field	13.5 MW	10.2 MW	10.2 MW	12.7 MW	45.4 MW
OTSI threshold field	0.26 V/m	0.22 V/m	0.21 V/m	0.21 V/m	0.46 V/m
Equivalent ERP of OTSI threshold field	64.7 MW	51.1 MW	43.2 MW	43.6 MW	163.8 MW

3.2. Excitation Threshold

Excitation of parametric instability requires that the parallel electric field of the heating wave exceeds the threshold electric field. Here we introduce the expressions of the threshold field for PDI and OTSI excitation in the ionospheric heating [*Wang et al.*, 2016]. These expressions are derived under the condition that the heating wave propagates along the magnetic field and the diagnostic radar beam also points along the magnetic field with a small angle (~0°):

$$E^2_{\mathrm{OTSIth}} = \frac{4m_e m_i}{e^2}\frac{c_s^2\omega_0^3\upsilon_e}{\left(\omega_0^2+\omega_{pe}^2\right)} \tag{9}$$

$$E^2_{\mathrm{PDIth}} = \frac{4m_i m_e}{e^2 k}\frac{\omega_0^3 c_s \upsilon_e \upsilon_i}{\left(\omega_0^2+\omega_{pe}^2\right)}, \tag{10}$$

where m_e, m_i, and e are the electron mass, ion mass, and electron charge, respectively. $c_s = \sqrt{k_b(T_e+3T_i)/m_i}$ is the ion acoustic velocity, $\Omega_e = eB_0/m_e$, and $\omega_{pe} = \sqrt{e^2 n_0/\varepsilon_0 m_e}$. B_0 is the geomagnetic strength. T_e and T_i are the background electron temperature and ion temperature. n_0 is the background electron density. k is wave number of the excited electrostatic wave. k_b is the Boltzmann constant. ε_0 is free space permittivity. $\upsilon_e = \upsilon_{ei}+\upsilon_{en}+\upsilon_{eL}$ and $\upsilon_i = \upsilon_{ie}+\upsilon_{in}+\upsilon_{iL}$ are the electron and ion effective collision frequency, respectively, where υ_{ei}, υ_{en}, υ_{ie}, and υ_{in} are electron-ion, electron-neutral, ion-electron, and ion-neutral collision frequencies respectively; electron and ion Landau damping are represented as [*Baumjohann and Treumann*, 1996]:

$$\upsilon_{eL} = \omega\sqrt{\pi/8}\Lambda_0^{3/2}(\eta_e)\exp\left[-1.5-\Lambda_0(\eta_e)/2k^2\lambda_D^2\right]/\left(k^2\lambda_D^3\right) \tag{11}$$

$$\upsilon_{iL} = \Delta\omega\sqrt{\pi/8}\left[(m_e/m_i)^{1/2}+(T_e/T_i)^{3/2}\exp(-T_e/2T_i-3/2)\right], \tag{12}$$

where $\Lambda_0(\eta_e) = I_0(\eta_e)\exp(-\eta_e)$, $\eta_e = k_\perp^2 v_{Te}^2/2\Omega_e^2$, I is modified Bessel function, and $\lambda_D = (\varepsilon_0 k_b T_e/n_0 e^2)^{1/2}$ is the electron Debye length. It should be noted that the equation (11) and equation (8) have self-consistency, because both can be obtained from the modified bi-Maxwellian distribution function.

By employing equations (9) and (10), Table 2 presents the threshold of the parallel electric field for exciting the parametric instability at the reflection heights of the *X*-mode heating wave for the three cases. The unperturbed background electron density, electron temperature, and ion temperature are obtained directly from the EISCAT UHF radar measurements (http://www.eiscat.se/madrigal) during the heater off cycle, as shown in Table 3. The neutral and collisions are obtained from NRLMSISE-00 [*Picone et al.*, 2002], and the geomagnetic field is obtained from the International Geomagnetic Reference Field (IGRF11) [*Finlay et al.*, 2010].

Table 3. The Ionospheric Parameters at the Interaction Height

Experiments	Case 1	Case 2		Case 3	
Heating wave frequency	7.1 MHz	6.2 MHz	5.423 MHz	7.1 MHz	5.423 MHz
Electron density (m^{-3})	5.06×10^{11}	3.73×10^{11}	2.74×10^{11}	5.06×10^{11}	2.74×10^{11}
Electron temperature (K)	1250	1170	1210	1690	1510
Ion temperature (K)	1045	1130	1070	890	870
Electron-ion collision frequency (1/s)	623.8	509.7	355.2	400.0	250.8
Electron Landau damping rate (1/s)	0.003	0.3	144.0	1.85	2.44×10^3
Ion Landau damping rate (1/s)	6.13×10^3	5.48×10^3	5.85×10^3	8.5×10^3	7.89×10^3

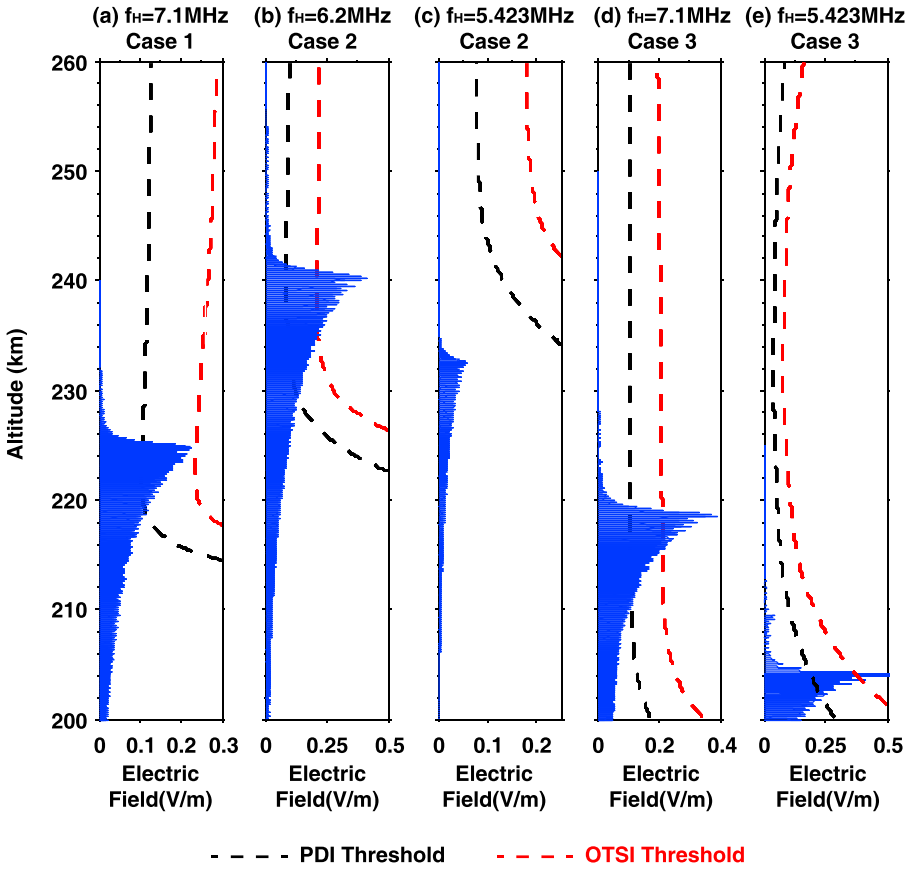

Figure 4. The equivalent parallel electric field of the pump wave near the reflection height of *X*-mode pump wave (a) $f_H = 7.1$ MHz in case 1, (b) $f_H = 6.2$ MHz in case 2, (c) $f_H = 5.423$ MHz in case 2, (d) $f_H = 7.1$ MHz in case 3, and (e) $f_H = 5.423$ MHz in case 3, where f_H is the heating wave frequency; the black dashed line and red dashed line mark the threshold field of PDI and OTSI, respectively.

The strong HFPLs and HFILs at the reflection height of the *X*-mode heating wave present direct evidence of the parametric instability excitation by the *X*-mode heating waves. Although it was thought that the parallel electric field at *X*-mode reflection height is too negligible to exceed the excitation threshold of parametric instability, we suggest that parallel electric field can still exceed the excitation threshold according to the observational facts. Based on experimental measurements, we calculate the parallel electric field at the reflection region of *X*-mode heating wave for the three experiments based on 1-D full-wave model [*Eliasson*, 2008; *Cannon and Honary*, 2015]. In our simulations, the heating wave propagates along the magnetic field as the experiments setting, i.e., the incident angle is 12° to vertical direction. Figure 4 presents the numerical simulation results for the three cases. Figures 4a–4e are the equivalent parallel electric field of *X*-mode heating wave near the reflection height at 7.1 MHz for the case 1, 6.2 MHz for the case 2, 5.423 MHz for the case 2, 7.1 MHz for the case 3, and 5.423 MHz for the case 3, respectively. Black and red dash lines mark the PDI threshold and OTSI threshold listed in Table 1, respectively. Figure 4a suggests that only PDI was excited in case 1. Parametric instability is not excited at 5.423 MHz heating wave frequency in case 2 as shown in Figure 4c. In another three experiments, shown in Figures 4b, 4d, and 4e, OTSI has been excited by *X*-mode heating wave. Simulation results are consistence with the experimental observations in section 2.

As mentioned in section 2.1, the EISCAT heating facility cannot absolutely separate the *O*-mode from *X*-mode wave, so it is probable for the leakage of *X*-mode power to *O* mode. *Blagoveshchenskaya et al.* [2014] suggested that less than 1% of full ERP could be leaked to *O*-mode wave under *X*-mode heating wave. In Case 1, both the HFPLs and HFILs at *O*-mode reflection height are observed during the *X*-mode heating sequence, which indicates that the *O*-mode wave excites the parametric instability. It implies that the electric field of *O*-mode leakage is more than 0.12 V/m, i.e., at least 2%–3% ERP of *X*-mode leakage to *O* mode. In Cases 2 and 3,

the HFPLs and HFILs at the *O*-mode reflection point are not observed during *X*-mode heating cycle. This indicates that the *O*-mode leakage cannot excite the parametric instability, because the electric field of *O*-mode leakage is less than the threshold field of the parametric instability. Therefore, the electric field of *O*-mode leakage is estimated to be less than 0.10 V/m, i.e., less than 2% ERP of *X*-mode leakage to *O* mode in these two cases.

Another point should be mentioned is that no upper hybrid waves are observed in our reported observations. *Vas'kov and Ryabova* [1998] calculated that the threshold of UH PDI excitation achieves 1.35 V/m under the condition of $\omega_0/\Omega_e = 4.5$. For the experiment of 19 October 2012, the condition is quite near to that of *Vas'kov and Ryabova* [1998], i.e., $\omega_0/\Omega_e \approx 4.5$. According to our calculation, the total equivalent electric field is about 0.66 V/m, which is much less than the UH PDI excitation threshold. Consequently, no UH wave observed in the experiment.

4. Summary

We have investigated the parametric instability excited by *X*-mode EM heating wave with EISCAT heating facility at Tromsø, Norway. Three experimental observations provide direct evidence for the parametric instability excitation by *X*-mode heating wave during ionospheric modification experiments. Strong HF-enhanced plasma lines at the reflection height of the *X*-mode heating wave associated with corresponding HF-enhanced ion lines are observed. Zero-frequency offset HFILs are also observed on the 19 October 2012 and 21 February 2013 experiments, which is a signature of the excitation of OTSI. The principal conclusions of our study can be summarized as follows.

1. HFPLs and HFILs observed at the reflection height of the *X*-mode heating wave provide direct evidence that the PDI or OTSI was excited during the *X*-mode heating periods.
2. A full Langmuir wave dispersion relation is suggested for parametric instability excited by *X*-mode heating wave to satisfy the frequency matching condition. In this paper, the modified bi-Maxwellian distribution function of the electron velocity is adopted to explain the frequency matching condition.
3. *X*-mode EM heating wave can excite Langmuir parametric instability near its reflection altitude. Our simulation results demonstrate that the parallel component of electric field of *X*-mode heating wave near the reflection height can also exceed the threshold of parametric instability under certain circumstance. Therefore, *X*-mode heating wave can also excite both the PDI and the OTSI.

Acknowledgments
EISCAT is an international scientific association supported by research organizations in China (CRIRP), Finland (SA), Japan (NIPR and STEL), Norway (NFR), Sweden (VR), and the United Kingdom (NERC). This work was supported by the National Natural Science Foundation of China (NSFC grants 41204111 and 41574146). X.W. appreciate the support by China Scholarship Council (201406270061). C.Z. appreciates the support by Wuhan University "351 Talents Project". The data used in this paper are available through the EISCAT Madrigal database (http://www.eiscat.se/madrigal/).

References

Ashrafi, M., M. J. Kosch, K. Kaila, and B. Isham (2007), Spatiotemporal evolution of radio wave pump-induced ionospheric phenomena near the fourth electron gyroharmonic, *J. Geophys. Res.*, *112*, A05314, doi:10.1029/2006JA011938.

Baumjohann, W., and R. A. Treumann (1996), *Basic Space Plasma Physics*, Imperial College Press, London.

Bernhardt, P. A., C. A. Tepley, and L. M. Duncan (1989), Airglow enhancements associated with plasma cavities formed during ionospheric heating experiments, *J. Geophys. Res.*, *94*, 9071–9092, doi:10.1029/JA094iA07p09071.

Blagoveshchenskaya, N. F., T. D. Borisova, T. Yeoman, M. T. Rietveld, I. M. Ivanova, and L. J. Baddeley (2011), Artificial field-aligned irregularities in the high-latitude *F* region of the ionosphere induced by an *X*-mode HF heater wave, *Geophys. Res. Lett.*, *38*, L08802, doi:10.1029/2011GL046724.

Blagoveshchenskaya, N. F., T. D. Borisova, T. K. Yeoman, M. T. Rietveld, I. Häggström, and I. M. Ivanova (2013), Plasma modifications induced by an *X*-mode HF heater wave in the high latitude *F* region of the ionosphere, *J. Atmos. Sol. Terr. Phys.*, *105-106*, 231–244, doi:10.1016/j.jastp.2012.10.001.

Blagoveshchenskaya, N. F., T. D. Borisova, M. Kosch, T. Sergienko, U. Brändström, T. K. Yeoman, and I. Häggström (2014), Optical and ionospheric phenomena at EISCAT under continuous *X*-mode HF pumping, *J. Geophys. Res. Space Physics*, *119*, 10,483–10,498, doi:10.1002/2014JA020658.

Brambilla, M. (1998), Kinetic theory of plasma waves: Homogeneous plasmas (No. 96) Oxford Univ. Press.

Cannon, P., and F. Honary (2015), A finite difference time domain scheme for electromagnetic wave interaction with plasma, *IEEE Trans. Antennas Propag.*, *63*(6), 3042–3054, doi:10.1109/TAP.2015.2423710.

DuBois, D. F., H. A. Rose, and D. Russell (1990), Excitation of strong Langmuir turbulence in plasmas near critical density: Application to HF heating of the ionosphere, *J. Geophys. Res.*, *95*, 21,221–21,272, doi:10.1029/JA095iA12p21221.

Eliasson, B. (2008), Full-scale simulation study of the generation of topside ionospheric turbulence using a generalized Zakharov model, *Geophys. Res. Lett.*, *35*, L11104, doi:10.1029/2008GL033866.

Fejer, J. A. (1979), Ionospheric modification and parametric instabilities, *Rev. Geophys.*, *17*(1), 135–153, doi:10.1029/RG017i001p00135.

Fejer, J. A., and E. Leer (1972), Excitation of parametric instabilities by radio waves in the ionosphere, *Radio Sci.*, *7*(4), 481–491, doi:10.1029/RS007i004p00481.

Fialer, P. A. (1974), Field-aligned scattering from a heated region of the ionosphere—Observations at HF and VHF, *Radio Sci.*, *9*(10), 923–940, doi:10.1029/RS009i011p00923.

Finlay, C. C., et al. (2010), International geomagnetic reference field: The eleventh generation, *Geophys. J. Int.*, *183*(3), 1216–1230, doi:10.1111/j.1365-246X.2010.04804.x.

Freund, H., and K. Papadopoulos (1980), The oscillating two stream and parametric decay instabilities in a weakly magnetized plasma, *Phys. Fluids*, *23*(1), 139–146, doi:10.1063/1.862854.
Ginzburg, V. L. (1970), *The Propagation of Electromagnetic Waves in Plasmas*, Elsevier, New York.
Gondarenko, N. A., S. L. Ossakow, and G. M. Milikh (2006), Nonlinear evolution of thermal self-focusing instability in ionospheric modifications at high latitudes: Aspect angle dependence, *Geophys. Res. Lett.*, *33*, L16104, doi:10.1029/2006GL025916.
Grach, S. M., and V. Y. Trakhtengerts (1975), Parametric excitation of ionospheric irregularities extended along the magnetic field, *Radiophys. Quantum Electron.*, *18*(8), 951–957, doi:10.1007/BF01038190.
Gurevich, A. V. (2007), Nonlinear effects in the ionosphere, *Phys.-Usp.*, *50*, 1091–1121, doi:10.1070/PU2007v050n11ABEH006212.
Gurevich, A. V., H. Carlson, Y. V. Medvedev, and K. R. Zybin (2004), Langmuir turbulence in ionospheric plasma, *Plasma Phys. Rep.*, *30*, 995–1005, doi:10.1134/1.1839953.
Honary, F., T. Robinson, D. Wright, A. Stocker, M. Rietveld, and I. McCrea (1999), First direct observations of the reduced striations at pump frequencies close to the electron gyroharmonics, *Ann. Geophys.*, *17*, 1235–1238.
Kosch, M. J., M. T. Rietveld, A. J. Kavanagh, C. Davis, T. K. Yeoman, F. Honary, and T. Hagfors (2002), High-latitude pump-induced optical emissions for frequencies close to the third electron gyro-harmonic, *Geophys. Res. Lett.*, *29*(23), 2112, doi:10.1029/2002GL015744.
Kosch, M. J., T. Pedersen, M. T. Rietveld, B. Gustavsson, S. M. Grach, and T. Hagfors (2007a), Artificial optical emissions in the high latitude thermosphere induced by powerful radio waves: An observational review, *Adv. Space Res.*, *40*, 365–376, doi:10.1016/j.asr.2007.02.061.
Kosch, M. J., T. Pedersen, E. Mishin, S.-I. Oyama, J. Hughes, A. Senior, B. Watkins, and B. Bristow (2007b), Coordinated optical and radar observations of ionospheric pumping for a frequency pass through the second electron gyro-harmonic at HAARP, *J. Geophys. Res.*, *112*, A06325, doi:10.1029/2006JA012146.
Kosch, M. J., T. Pedersen, E. Mishin, M. Starks, E. Gerken-Kendall, D. Sentman, S. Oyama, and B. Watkins (2007c), Temporal evolution of pump beam self-focusing at the High-Frequency Active Auroral Research Program, *J. Geophys. Res.*, *112*, A08304, doi:10.1029/2007JA012264.
Kuo, S. (1996), The role of nonlinear beating currents on parametric instabilities in magnetoplasmas, *Phys. Plasmas*, *3*, 3957, doi:10.1063/1.871568.
Kuo, S. (2002), Oscillating two-stream instability in ionospheric heating experiments, *Phys. Plasmas*, *9*(4), 1456–1459, doi:10.1063/1.1453471.
Kuo, S. (2015), Ionospheric modifications in high frequency heating experiments, *Phys. Plasmas*, *22*, 012901, doi:10.1063/1.4905519.
Lee, M., and S. Kuo (1983), Excitation of upper-hybrid waves by a thermal parametric instability, *J. Plasma Phys.*, *30*(3), 463–478, doi:10.1017/S002237780000129X.
Lehtinen, M. S., and A. Huuskonen (1996), General incoherent scatter analysis and GUISDAP, *J. Atmos. Sol. Terr. Phys.*, *58*, 435–452, doi:10.1016/0021-9169(95)00047-X.
Leyser, T. B., and A. Y. Wong (2009), Powerful electromagnetic waves for active environmental research in geospace, *Rev. Geophys.*, *47*, RG1001, doi:10.1029/2007RG000235.
Minkoff, J., P. Kugelman, and I. Weissman (1974), Radio frequency scattering from a heated ionospheric volume: 1, VHF/UHF field-aligned and plasma-line backscatter measurements, *Radio Sci.*, *9*(10), 941–955, doi:10.1029/RS009i011p00941.
Mishin, E., H. C. Carlson, and T. Hagfors (2000), On the electron distribution functionin the *F* region and airglow enhancements during HF modification experiments, *Geophys. Res. Lett.*, *27*, 2857–2860, doi:10.1029/2000GL000075.
Mishin, E., B. Watkins, N. Lehtinen, B. Eliasson, T. Pedersen, and S. Grach (2016), Artificial ionospheric layers driven by high-frequency radiowaves: An assessment, *J. Geophys. Res. Space Physics*, *121*, 3497–3524, doi:10.1002/2015JA021823.
Pedersen, T., and H. Carlson (2001), First observations of HF heater-produced airglow at the High Frequency Active Auroral Research Program facility: Thermal excitation and spatial structuring, *Radio Sci.*, *36*, 1013–1026, doi:10.1029/2000RS002399.
Pedersen, T., B. Gustavsson, E. Mishin, E. MacKenzie, H. C. Carlson, M. Starks, and T. Mills (2009), Optical ring formation and ionization production in high-power HF heating experiments at HAARP, *Geophys. Res. Lett.*, *36*, L18107, doi:10.1029/2009GL040047.
Perkins, F. W., C. Oberman, and E. J. Valeo (1974), Parametric instabilities and ionospheric modification, *J. Geophys. Res.*, *79*(9), 1478–1496, doi:10.1029/JA079i010p01478.
Picone, J. M., A. E. Hedin, D. P. Drob, and A. C. Aikin (2002), NRLMSISE-00 empirical model of the atmosphere: Statistical comparisons and scientific issues, *J. Geophys. Res.*, *107*(A12), 1468, doi:10.1029/2002JA009430.
Robinson, T. R. (1989), The heating of the high latitude ionosphere by high power radio wave, *Phys. Rep.*, *179*, 79–209, doi:10.1016/0370-1573(89)90005-7.
Senior, A., M. T. Rietveld, M. J. Kosch, and W. Singer (2010), Diagnosing radio plasma heating in the polar summer mesosphere using cross modulation: Theory and observations, *J. Geophys. Res.*, *115*, A09318, doi:10.1029/2010JA015379.
Senior, A., M. T. Rietveld, I. Häggström, and M. J. Kosch (2013), Radio-induced incoherent scatter ion line enhancements with wide altitude extents in the high-latitude ionosphere, *Geophys. Res. Lett.*, *40*, 1669–1674, doi:10.1002/grl.50272.
Stubbe, P., H. Kopka, and B. Thide (1984), Stimulated electromagnetic emission: A new technique to study the parametric decay instability in the ionosphere, *J. Geophys. Res.*, *89*, 7523–7536, doi:10.1029/JA089iA09p07523.
Stubbe, P., H. Kohl, and M. T. Rietveld (1992), Langmuir turbulence and ionospheric modification, *J. Geophys. Res.*, *97*, 6285–6297, doi:10.1029/91JA03047.
Thome, G. D., and D. W. Blood (1974), First observations of RF backscatter from field-aligned irregularities produced by ionospheric heating, *Radio Sci.*, *9*(10), 917–921, doi:10.1029/RS009i011p00917.
Utlaut, W. F., and R. Cohen (1971), Modifying the ionosphere with intense radio waves, *Science*, *174*(4006), 245–254, doi:10.1126/science.174.4006.245.
Vas'kov, V. V., and N. A. Ryabova (1998), Parametric excitation of high frequency plasma oscillations in the ionosphere by a powerful extraordinary radio wave, *Adv. Space Res.*, *21*, 697–700, doi:10.1016/S0273-1177(97)01006-5.
Wang, X., P. Cannon, C. Zhou, F. Honary, B. Ni, and Z. Zhao (2016), A theoretical investigation on the parametric instability excited by X-mode polarized electromagnetic wave at Tromsø, *J. Geophys. Res. Space Physics*, *121*, 3578–3591, doi:10.1002/2016JA022411.